chemistry

MDPI

Article

CIGS Electrodeposition from Diluted Electrolyte: Effect of Current Density and Pulse Timing on Deposition Quality and Film Properties

Mahfouz Saeed

Energy and Sustainable Engineering Deptartment, College of Engineering, A'Sharqiyah University, P.O. Box 42, Ibra 400, Oman; mahfouz.saeed@asu.edu.om

Abstract

Among the most promising alloys for photovoltaic applications is copper–indium–gallium–selenide (CIGS) because of its enhanced optical properties. This study examines the influence of current density and pulse timing on the electrodeposition of Cu(In, Ga)Se_2 (CIGS) thin films from a dilute electrolyte. It assesses how these parameters affect deposition quality, film characteristics, and device performance. CIGS absorber layers were electrodeposited using a pulsed-current method, with systematic variations in current density and pulse on/off durations in a low-concentration solution. The deposited precursors were subsequently selenized and incorporated into fully assembled CIGS solar cell architectures. Structural characteristics were analyzed by X-ray diffraction (XRD), whereas composition and elemental distribution were assessed by energy-dispersive X-ray spectroscopy (EDS). Optical properties pertinent to photovoltaic performance were evaluated through transmittance and reflectance measurements. The results indicate that moderate current densities, when combined with brief off-times, produce dense, microcrack-free films exhibiting enhanced crystallinity and near-stoichiometric Cu/(In + Ga) and Ga/(In + Ga) ratios, in contrast to films deposited at higher current densities and extended off-times. These optimized pulse parameters also produce absorber layers with advantageous optical band gaps and improved device performance. Overall, the study demonstrates that regulating pulse parameters in attenuated electrolytes is an effective strategy to optimize CIGS film quality and to facilitate the advancement of economical, solution-based fabrication methods for high-performance CIGS solar cells.

Keywords: CIGS; photovoltaic; electrodeposition; pulsing current; thin film; hydrogen evolution; PV cells

Check for updates

Academic Editor: Michael Lyons

Received: 25 November 2025
Revised: 1 January 2026
Accepted: 5 January 2026
Published: 8 January 2026

Copyright: © 2026 by the author. Licensee MDPI, Basel, Switzerland. This article is an open access article distributed under the terms and conditions of the Creative Commons Attribution (CC BY) license.

1. Introduction

CuInxGa$_{(1-x)}$$Se_2$ (CIGS) is a solar thin-film quaternary compound composed of copper, indium, gallium, and selenium. CIGS serves as an ideal absorber layer for photovoltaic (PV) devices. The variable 'x' in the equation may yield any value within the range of 0 to 1. It significantly affects the CIGS structure and its band gap energy [1]. Specific individuals assert that the optimal x value is 0.3 [1]. The CIGS thin film must be 1.5–2.5 µm thick. This film is suitable for solar applications due to its high optical absorption coefficient of approximately 10^5 cm^{-1} [2].

Numerous research teams have examined the growth mechanisms of the CIGS device absorber operating layer and the chemistry of the electrodeposition solution. Individuals

are becoming more interested in non-vacuum methods for making CIGS films, as they are cheaper to produce and easier to scale up for large areas [3–6]. Among these, making CIGS thin layers by electrodeposition is particularly appealing, as it requires minimal setup and can produce multiple layers quickly [7–9]. The hybrid technique, which combined electrodeposition with gas-phase species addition, produced a device with 10.9% efficiency [10]. Adding pHydrion buffer—a solution of potassium biphthalate and sulfamic acid—to the solution composition has proven very useful for removing indium and gallium oxides and hydroxides, thereby stabilizing the absorber layer [10–12]. Non-vacuum methods for producing CIGS films are gaining attention due to their significantly lower production costs and enhanced scalability for large-area fabrication [13]. The manufacture of CIGS thin-film devices via electroplating is particularly attractive due to its comparatively high throughput and low investment [14–17]. The hybrid technique, which integrates electrodeposition with gas-phase metal addition, yielded a device with an efficiency of 15.4% [18]. The incorporation of pHydrion buffer, a combination of potassium biphthalate and sulfamic acid, into the electrodeposition solution has significantly reduced the concentration of gallium and indium oxides and hydroxide compounds, resulting in a resilient absorber layer [19,20]. Nickel, followed by a molybdenum layer, has been identified as a suitable back contact due to its high electrical conductivity. Similarly, a study has examined the roughness of electrodeposited CIGS on several back contacts, including molybdenum, copper, and fluorine-doped tin oxide [21].

Furthermore, the electrochemical deposition of CIGS has been investigated on the ZnO window layer. Electroplating of copper, indium, and gallium was subsequently followed by the addition of selenium during annealing, as documented in references [22–24]. A study on the electrodeposition of CIGS on structured molybdenum/glass substrates demonstrated that it can be used as a semi-transparent photovoltaic cell for glazing [24]. Several research teams have focused on understanding the chemistry of the electrodeposition solution and the mechanisms underlying the fabrication of CIGS absorbers. The film generated by low-temperature electrodeposition exhibits low crystallinity and requires subsequent thermal treatment (annealing) [24–28]. The literature recommends annealing in a selenium atmosphere to facilitate interactions between selenium and copper, gallium, and indium, thereby promoting formation processes, effective recrystallization, and optimizing the final composition of the absorber [27–30].

Furthermore, investigations into the post-thermal-treatment process of CIGS indicate that this phase significantly influences the photovoltaic cell's efficiency due to the impact on the grain size and crystal structure of the CIGS alloy, thereby enhancing light absorption [31]. Film structure can also be influenced by the precursor type and the Cu/In atomic ratio [32]. Pulse electrodeposition has been proposed to achieve a good CIGS layer and enhance control throughout the electroplating process [33–35]. The electrodeposition technique, succeeded by physical vapor deposition, incorporates a vapor stage of copper, indium, and gallium into the CIGS main layer, as documented [36]. Comprehensive research on CIGS electrodeposition procedures has been reported in the literature, except for hydrogen evolution [37–39].

To clarify the electrochemical production procedures of its four metals, the CIGS system has been primarily examined using potential-sweep techniques. Recent research has examined the electrodeposition of CIGS on a rotating disc electrode (RDE) using two different approaches: DC electrodeposition and DC electrodeposition combined with mechanical perturbations [40–43]. Moreover, extensive research has been conducted on RDE in the copper–indium–selenium (CIS) system. There is insufficient information available on the importance of agitation and mass transport in CIGS electroplating, as most published studies on the subject were conducted in beakers under poorly specified transport conditions.

In conclusion, although CIGS electrodeposition has been studied for approximately three decades, few researchers recognize the critical roles that agitation and mass transport play in the CIGS electroplating process, which is a crucial component for achieving a well-controlled absorption layer with a consistent atomic ratio of the target alloy across a large field scale. Likewise, it is essential to recognize that synthesizing the CIGS alloy requires the application of large overpotentials and that the reduction in protons to produce hydrogen gas significantly affects the alloy film's ultimate composition and shape. However, no studies have been published to date that clarify the mechanisms governing mass transfer and/or reaction kinetics using the pulsing technique, which separately regulates each precursor during CIGS alloy development, despite the significant issue of hydrogen gas co-evolution. Therefore, these essential problems can be described as a dilemma that previous research has overlooked; this suggests that the focus of this study is the substantial amount of hydrogen gas generated during CIGS deposition, as well as the mass-transport effect during alloy deposition [7]. The use of the rotating disk electrode to characterize the significance of transport in CIGS electrodeposition is methodically investigated in this work under pulsing current. To ensure uniform, precisely defined transport rates throughout the electrode, the RDE provides a quantitative evaluation of agitation speeds, which play a role in the disk's rotation device.

The primary goal of this study was not to achieve maximum efficiency. Instead, the focus was on a systematic investigation of how diluted electrolyte composition, current density, and pulse timing affect film growth, morphology, and composition. Furthermore, the objective was to demonstrate the feasibility of producing reasonably functional devices under these simplified and diluted conditions.

In our previous publications, CIGS was deposited from comparatively concentrated electrolytes. In the present study, we deliberately utilize an electrolyte that is ten times more reduced than in conventional investigations, and we examine whether such a low-ion-strength solution can still produce dense, stoichiometric absorbers appropriate for device fabrication. To the best of our knowledge, this represents the initial systematic investigation of CIGS absorber electrodeposition employing a highly attenuated electrolyte in conjunction with pulse current deposition.

In this study, we use a similar system to the diluted system previously used, resulting in noticeably improved deposit properties [7]. Additionally, by evaluating the hydrogen current density relative to the precursor current density and the overall current density during alloy reduction, the role of hydrogen co-evolution in the electrodeposition of CIGS is examined.

Along with the CIGS absorber layer, a complete photovoltaic device was fabricated solely by electrodeposition. This device has the following layers: stainless steel/Ni/Mo/CIGS/CdS/ZnO/ZnO-Al. To characterize the integrated photovoltaic device, we measured its quantum efficiency using a solar simulator. The characteristics characterized include the fill factor, band gap, open-circuit voltage, short-circuit current, and overall efficiency.

2. Specifics of the Experiment

Electrodeposition was performed utilizing a commercial rotating disc electrode (RDE) system A Bio-Logic USA potentiostat/galvanostat Model VSP, equipped with a motor controller to regulate the rotation speed of the working electrode and configured with a standard three-electrode electrochemical cell setup. The device included a 0.32 cm^2 stainless steel (406 SS) electrode coated with a 99.95% Mo molybdenum layer by electron-beam physical vapor deposition. The procedure was performed in a vacuum atmosphere with a pressure of 2×10^{-6} torr. To mitigate the effects of elevated temperatures on the equipment,

the deposition rate was reduced to 0.3 Å/s. Consequently, the sputtering procedure was conducted for 60 min to achieve a thickness of approximately one μm. The disk was then flush-embedded in an insulated Teflon cylinder, with a saturated calomel electrode (SCE) serving as the reference electrode and a platinum lattice as the counter electrode. A 50 mL beaker filled with the electrochemical solutions that were being investigated was submerged with the electrodes. Hydrochloric acid was introduced to regulate the electrolyte pH to 1.9. Rotation velocities of 0 to 700 rpm were employed during experiments conducted at an ambient temperature of 20 °C.

First, acetone was used to rinse the substrate, followed by deionized water and air drying. The substrate was electroactivated in 0.1 M sulfuric acid at 1.5 V vs. NHE for 2 s before electrodeposition. The traditional higher concentration chemical system was composed of 3.9–5.9 mM $CuCl_2 \cdot 2H_2O$ (Sigma-Aldrich, St. Louis, MO, USA), 3.1–5.1 mM $InCl_3$ (Strem-Chemicals, Newburyport, MA, USA), 6–10 mM H_2SeO_3 (Sigma-Aldrich), 2.8–6.2 mM $GaCl_3$ (Strem-Chemicals), pHydrion (pH = 2) (Sigma-Aldrich), and 0.71 M LiCl (Sigma-Aldrich) as the supporting electrolyte. The novel bath was a reduced-concentration system that included a supporting electrolyte of 0.66 M LiCl, pHydrion (pH = 2), 0.31–0.49 mM $InCl_3$, 0.5–0.79 mM H_2SeO_3, and 0.34–0.58 mM $GaCl_3$. To achieve the optimal film composition and performance, the electrolyte ranges listed above were investigated. The experiments were conducted potentiostatically, with electrodeposition potentials ranging from −0.62 V to −0.77 V vs. the standard hydrogen electrode (NHE). This indicates that the electrodeposition potential is equivalent to the reference electrode on the scale (0 V vs. NHE = 0.242 V vs. SCE).

In this research, the complete PV device was manufactured by electrodepositing additional layers on top of the CIGS film. The initial CdS layer, approximately 50 nanometres thick, was deposited on the CIGS absorber. The electrodeposition of cadmium sulfide was conducted at a temperature of 65 °C in an electrolyte that contained 0.2 M $CdCl_2$, 5 mM $Na_2S_2O_3$, and 0.5 M KCl. The bath was adjusted to 2 by adding HCl. The electrolyte was subjected to −0.8 V vs. SCE for 12 min. 190 nm of electroplated undoped zinc oxide transparent layer was deposited after the deposition of the CdS layer. Using an electrolyte comprising 0.1 M $Zn(NO_3)_2$ and 0.4 M KCl, this layer was electrodeposited for 40 min at 300 rpm and 75 °C by applying -0.85 V versus SCE. NaOH was added to bring the bath's pH down to 6. Finally, using an electrolyte comprising 0.1 M $Zn(NO_3)_2$, 0.9 mM $InCl_3$, and 0.4 M KCl, a 500 nm indium-doped zinc oxide window coating was deposited by applying −1.1 V versus SCE for 55 min at 200 rpm and 80 °C. Using NaOH, the pH buffer was brought to 3.5.

The final composition of the electrodeposit at the CIGS surface was analyzed using a Hitachi S4500 scanning electron microscope (SEM) (Hitachi, Tokyo, Japan) coupled with a Noran Energy Dispersive Spectrometer (EDS). A NORAN System SIX EDS detector (Thermo Fisher Scientific, Madison, WI, USA) that was integrated with a scanning electron microscope was used to gather EDS spectra. The atomic composition analysis of the CIGS film cross-section was conducted using a focused ion beam (FIB) technique on the FEI Helios NanoLab 650 Dual-Beam System fitted with an EDS. X-ray diffraction (XRD) was employed to analyze the crystallography of CIGS using a Bruker Discover D8 X-ray diffractometer, with Cu K alpha (α) radiation (λ = 0.15406 nm) as the source, and a step size of 0.01°. The equipment employed in the PV measurements consisted of the QEX10 quantum efficiency measurement system and an Oriel Sol2A solar simulator, Irvine, CA, USA. Consequently, the characterized parameters include overall efficiency, quantum efficiency, open-circuit voltage, short-circuit current, dark current, band gap, and fill factor.

3. Results and Discussion

3.1. Electrodeposition

3.1.1. Electrodeposition Using Pulsing Current

CIGS electrodeposition is complicated by the four elements' significant variations in typical deposition potentials. Because co-deposition must occur at a potential more negative than gallium's, the majority of species must deposit at their limiting current. Complex electrochemical processes employing selenium and a variety of chemical reactions produce metal selenides.

Polarization tests were conducted, as in previous studies, to explain the agitation effects and improve plating conditions at three different rotational rates (100, 300, and 500 rpm) [6,7]. The electrochemical behavior is associated with substantial hydrogen evolution. Moreover, about 50% of the plating current is hydrogen evolution. The electrochemical behaviour of the CIGS system equivalents is equivalent to that of the CIGS system discussed in our previous work [3]. Nevertheless, the current is diminished. By comparing experimental data with expected limiting currents for the four metals at various potentials, we established that selenium and copper are at their limiting currents. In contrast, indium and gallium are subject to kinetic regulation practically at pulsing current.

The introduction of a pulsing current facilitates the adjustment of the four species content in the final deposit composition, resulting in a smooth deposit from the previously specified diluted solution [3]. In a more diluted electrolytic solution, hydrogen evolution occurs less frequently than in the conventional solution concentration. Moreover, the less concentrated solution yielded a uniform, smooth, and exceedingly adhesive deposit.

As expected, the electrolyte with reduced concentration exhibited a significantly lower total deposition current compared to the system with high concentration, as illustrated in Figure 1 [3]. Furthermore, all four species exhibit behaviour governed by mass transfer (Figure 1) due to reduced concentrations, which influence their limiting current.

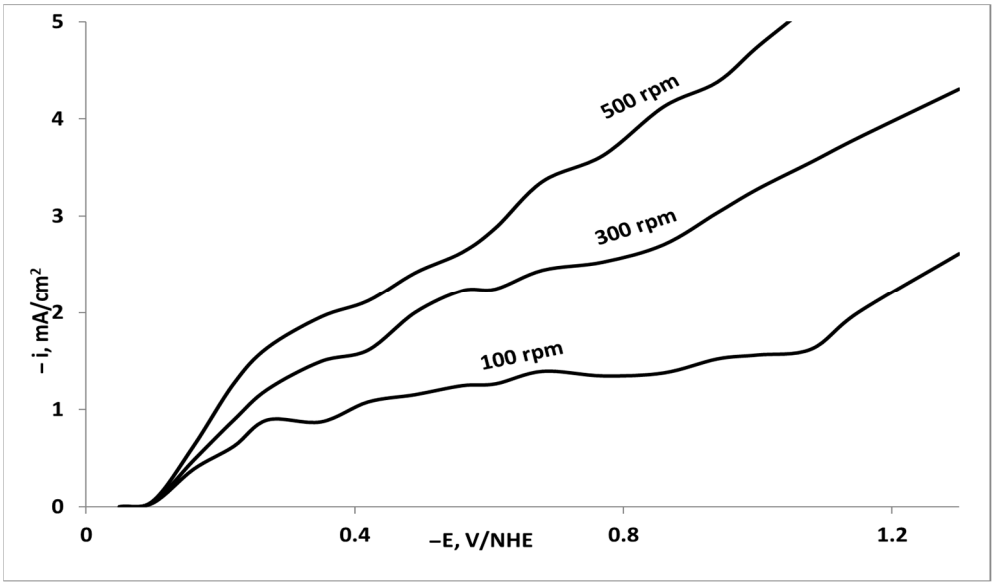


Figure 1. Polarization curves for CIGS deposition at different RDE rotation speeds (±1 standard deviation based on repeated measurements). The electrolyte from which the CIGS was deposited consisted of 0.47 mM $CuCl_2 \cdot H_2O$, 0.40 mM $InCl_3$, 0.71 mM H_2SeO_3, and 0.55 mM $GaCl_3$, supporting the bath. 0.65 M LiCl was added as a supporting electrolyte, and pHydrion was added to buffer the electrolyte to pH = 2.

3.1.2. Hydrogen Evolution

To characterize the amount of hydrogen evolution and to gain insights into the governing deposition regime of the individual components, partial current polarization curves were plotted by analyzing the sample composition (via EDS) and subsequently calculating the partial currents of each metal component based on their weight using Faraday's law. The polarization curves of the partial currents are displayed in Figure 2.

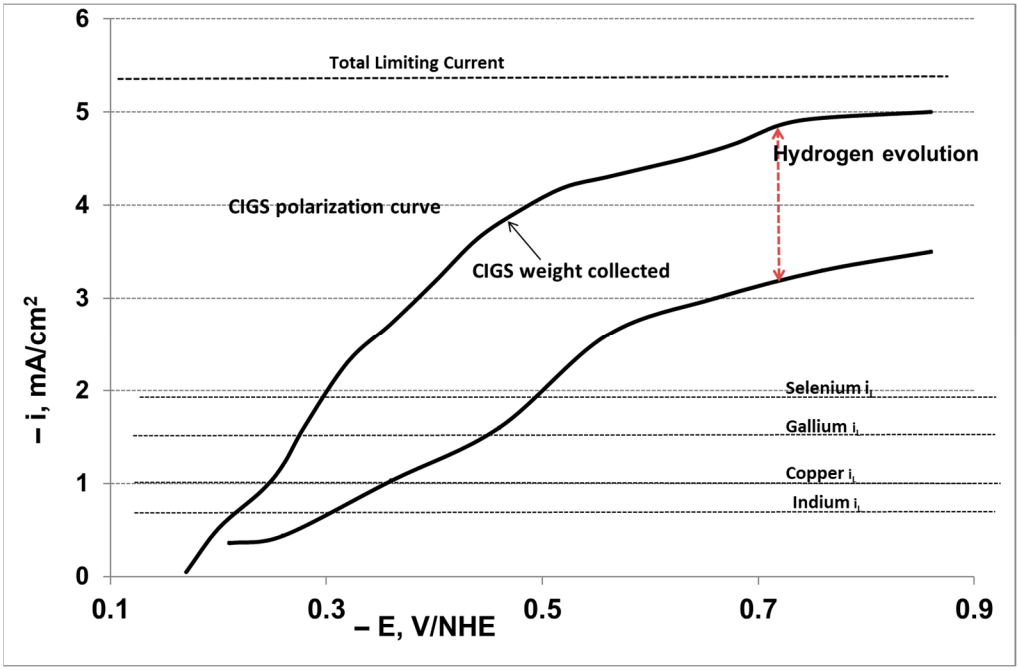


Figure 2. Limiting current polarization curves for CIGS deposition (collected vs. measured) (±1 standard deviation based on repeated measurements). The electrolyte from which the CIGS was deposited consisted of 0.47 mM $CuCl_2 \cdot H_2O$, 0.40 mM $InCl_3$, 0.71 mM H_2SeO_3, and 0.55 mM $GaCl_3$, supporting the bath. 0.65 M LiCl was added as a supporting electrolyte, and pHydrion was added to buffer the electrolyte to pH = 2.

The partial currents data were integrated to present the overall CIGS deposition current density, derived from the compositional analysis of the deposit, as illustrated in Figure 2. The discrepancy between the measured total current density and that derived from the compositional deposit analysis is attributed to hydrogen evolution. Additionally, Figure 2 illustrates the theoretical limiting current densities, i_L, calculated using the Levich equation presented below [3].

$$i_L = i_{Levich} = 0.62nFAD_j^{2/3}\omega^{1/2}v^{-1/6}C_{b,j} \quad (1)$$

Equation (1) represents the limiting current density on a rotating disk electrode under steady-state conditions. Here, ω represents the angular rotation rate (rad/s), v denotes the kinematic viscosity of the electrolyte (approximately 0.01 cm^2/s), and A refers to the geometric axial area of the working electrode, respectively. The quantity of evolved hydrogen in this system accounts for approximately 30% of the total current. This indicates that the morphology of the surface deposit may be influenced by hydrogen evolution and the concentration of metal ions, as these species compete for reduction at the electrode surface.

3.2. Electrodeposition of CIGS Film

A pulsed current of 4.2 mA/cm^2 was applied during CIGS electrodeposition, with 50-millisecond on and off intervals. For fifty minutes, the deposition experiments were

carried out at room temperature, or roughly 20 °C. The concentrations of the species were adjusted to get the desired final atomic composition of CIGS. The atomic composition was ascertained using the EDS method. Achieving the required selenium ratio in the finished film is difficult with a pulse current of under 2.75 mA/cm^2. The EDS elemental maps in Figure 3 show a relatively uniform lateral distribution of the four constituent elements across the analyzed region, with no apparent large-scale differentiation or depletion zones. The final mixture was synthesized after 35 min of annealing at 520 °C in an argon atmosphere. Figure 3 demonstrates that several substantial grains included metallic selenides.

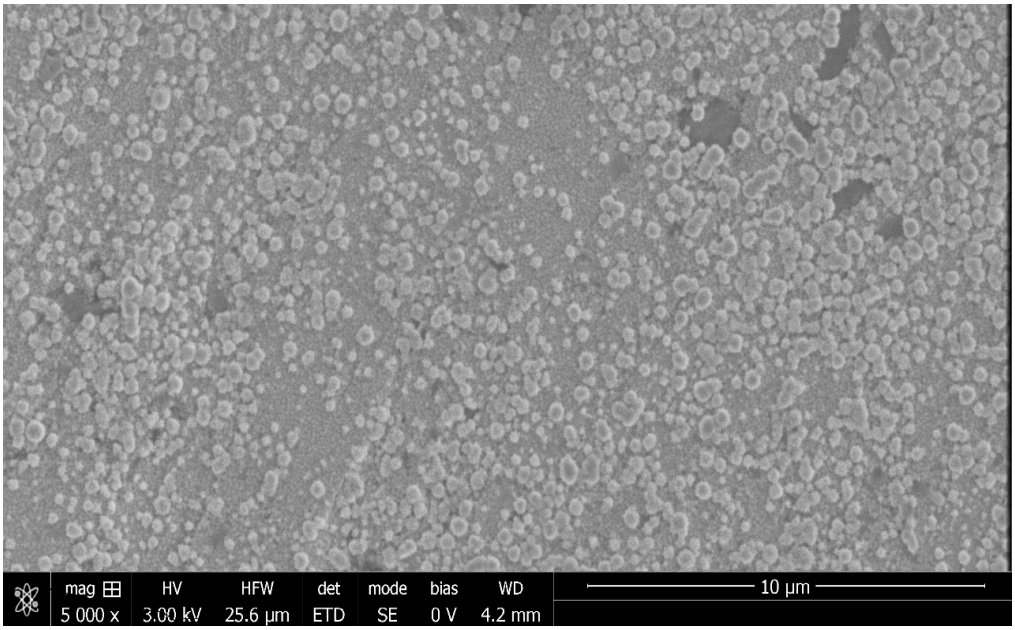


Figure 3. SEM photograph of CIGS film deposited from the dilute electrolyte. The electrolyte from which the CIGS was deposited consisted of 0.47 mM $CuCl_2 \cdot H_2O$, 0.40 mM $InCl_3$, 0.71 mM H_2SeO_3, and 0.55 mM $GaCl_3$, supporting the bath. 0.65 M LiCl was added as a supporting electrolyte, and pHydrion was added to buffer the electrolyte to pH = 2.

The surface and cross-sectional morphologies of the CIGS films were characterized using a field-emission scanning electron microscope (SEM) operated at 10–15 kV, a working distance of 8–10 mm, and a beam current of 1–2 nA. Images were primarily obtained in secondary electron (SE) mode under high-vacuum conditions, with magnifications ranging from 5000× to 50,000×.

Elemental analysis and compositional mapping were performed utilizing an energy-dispersive X-ray spectroscopy (EDS) system integrated with the SEM. EDS spectra and maps were acquired at an accelerating voltage of 15–20 kV, with a dwell time of 40–60 s and a take-off angle of approximately 35°. The acquisition area for surface mapping was typically 50 × 50 µm^2, with a pixel dwell time of 50–100 µs. Quantification was conducted employing a standardless ZAF correction method, and the reported compositions represent the average of multiple measurement points.

Elemental analysis and compositional mapping were performed utilizing an energy-dispersive X-ray spectroscopy (EDS) system integrated with the SEM. EDS spectra and maps were acquired at an accelerating voltage of 15–20 kV, with a dwell time of 40–60 s and a take-off angle of approximately 35°. The acquisition area for surface mapping was typically 50 × 50 µm^2, with a pixel dwell time of 50–100 µs. Quantification was conducted utilizing a standardless ZAF correction method, and the reported compositions represent the average of multiple measurement points.

Table 1 demonstrates the variation in solution composition and its effect on CIGS final atomic composition. The formulation of the baths comprising gallium chloride, indium chloride, selenious acid, and copper chloride has been modified. The resultant deposit composition was nearly aligned with the desired composition. The first four columns (on the left) of Table 1 present the chemical compositions that contributed to the roughly optimal final atomic composition. A 50 msec on and 50 msec off cycle yields a deposition pulsing current of 4.2 mA/cm^2. The remaining four columns enumerate the ultimate atomic compositions of the alloys.

Table 1. CIGS deposit final atomic composition after thermal treatment in an argon atmosphere.

					Composition [Atomic %]			
Bath (mM)	**$CuCl_2$**	**$GaCl_3$**	**$InCl_3$**	**H_2SeO_3**	**Cu**	**In**	**Ga**	**Se**
Bath 1	0.45	0.51	0.4	0.72	24.2	17.2	7.9	51.1
Bath 2	0.49	0.54	0.47	0.64	24.8	17.5	7.2	50.1
Bath 3	0.46	0.51	0.41	0.61	24.9	17.7	7.6	49.3

3.3. Grain Size and Morphology

Three samples with varying pulsing current density and timing were examined to determine the influence of the pulsing technique on the absorber layer morphology. The SEM study of the atomic deposit reveals that grain size is affected by the pulsing current. Figure 4 illustrates the initial sample, with 4.2 mA/cm^2 and 50 msec on and off, which was deposited under comparable conditions. In samples with short-pulsing current, the deposit exhibited a smooth texture and a relatively small surface grain size of about 300 nm, as observed by SEM. The electrodeposited CIGS was evenly distributed throughout the sample, as illustrated in Figure 4.

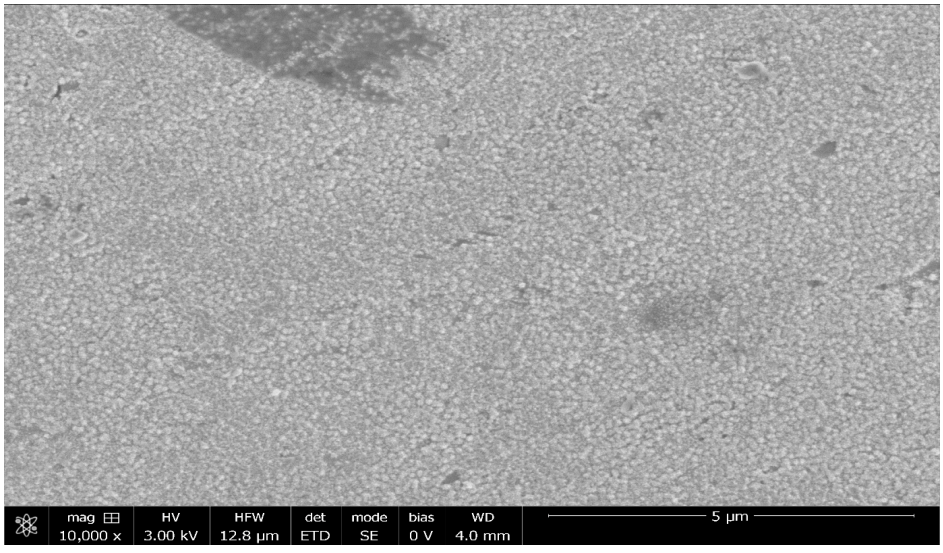


Figure 4. CIGS with short pulsing time at 500 rpm. The deposition pulsing current is 4.2 mA/cm^2 with 50 msec on and 50 msec off. The electrolyte from which the CIGS was deposited consisted of 0.47 mM $CuCl_2 \cdot H_2O$, 0.40 mM $InCl_3$, 0.71 mM H_2SeO_3, and 0.55 mM $GaCl_3$, supporting the bath. 0.65 M LiCl was added as a supporting electrolyte, and pHydrion was added to buffer the electrolyte to pH = 2.

Figure 4 illustrates the initial sample, with 5.3 mA/cm^2 and 100 msec on and off, which was deposited under comparable conditions. In this sample with a longer width

and current pulsing time, the deposit was rougher than in the previous sample, with a relatively limited distribution and a greater crystallized grain size (7 nm). This deposit provides continuous coverage of the sample surface with acceptable quality (Figure 5).

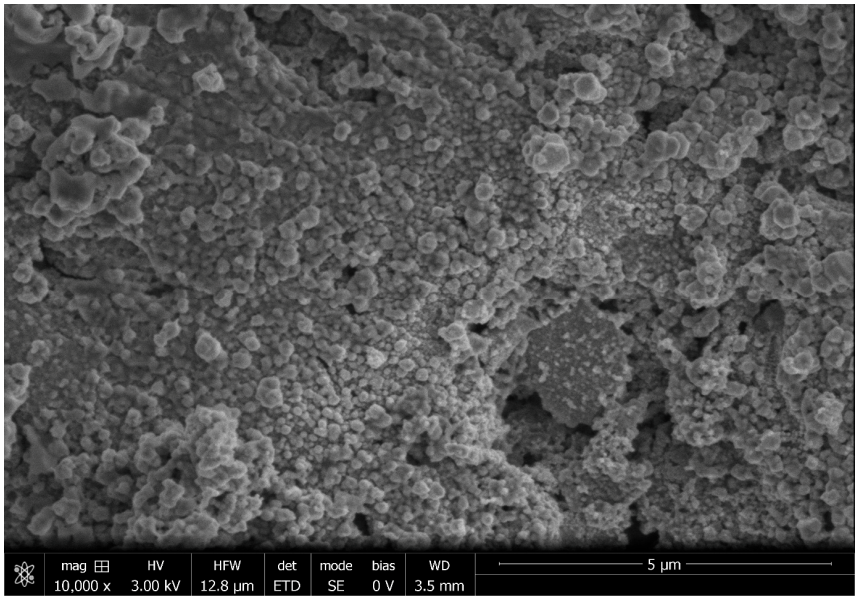


Figure 5. CIGS with medium pulsing current, deposited at 500 rpm. The deposition pulsing current was 3.9 mA/cm^2 with 100 msec on and 100 msec off. The electrolyte from which the CIGS was deposited consisted of 0.47 mM $CuCl_2 \cdot H_2O$, 0.40 mM $InCl_3$, 0.71 mM H_2SeO_3, and 0.55 mM $GaCl_3$, supporting the bath. 0.65 M LiCl was added as a supporting electrolyte, and pHydrion was added to buffer the electrolyte to pH = 2.

The third sample, shown in Figure 6, produced a deposit of 5.4 mA/cm^2, with 250 msec on and off, under comparable conditions. In this sample, with a longer width and current pulsing time, the deposit was rougher than in the previous samples, with a poor distribution and a greater grain size (15 nm). This deposit exhibits a coarse texture and uniformly covers the surface, as illustrated in Figure 6.

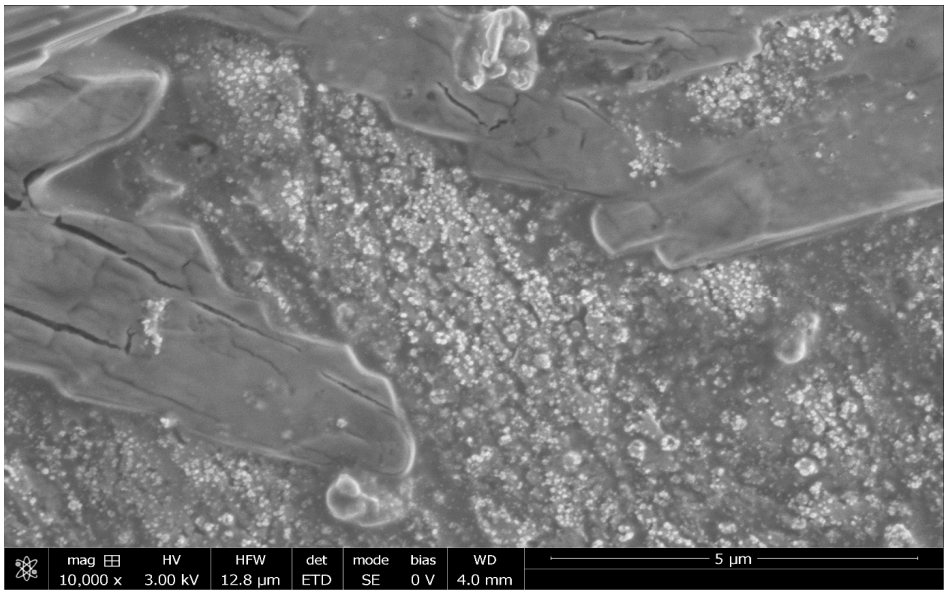


Figure 6. CIGS deposited at 500 rpm (long-pulsing current). The deposition pulsing current was 3.9 mA/cm^2 with 250 msec on and 250 msec off. The electrolyte from which the CIGS was deposited

consisted of 0.47 mM $CuCl_2 \cdot H_2O$, 0.40 mM $InCl_3$, 0.71 mM H_2SeO_3, and 0.55 mM $GaCl_3$, supporting the bath. 0.65 M LiCl was added as a supporting electrolyte, and pHydrion was added to buffer the electrolyte to pH = 2.

3.4. Deposit Analysis

The EDS analysis of the CIGS samples demonstrated a consistent composition of the four constituent metals in each sample, shown in Figure 7. Selenium demonstrated a steady atomic concentration at the designated levels prior to thermal post-treatment. Because it removes the necessity of adding selenium or indium from the vapor phase, this is a noteworthy accomplishment that could shorten the annealing time substantially (Figure 7).

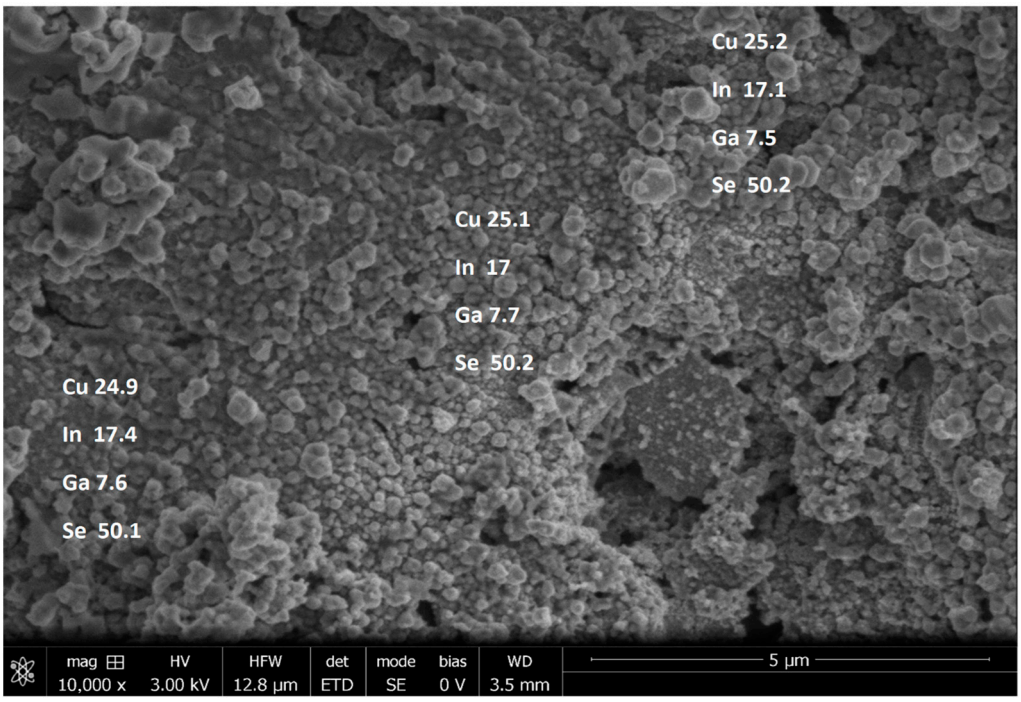


Figure 7. Surface composition of CIGS samples electroplated and analyzed via EDS. The atomic composition is relatively uniform across the sample.

EDS analysis was conducted at (10) randomly chosen locations on the surface of the CIGS absorber. The mean elemental composition was determined to be Cu 25.2 ± 0.8 atomic%, In 17.1 ± 0.6 atomic%, Ga 7.5 ± 0.4 atomic%, and Se 50.2 ± 1.1 atomic% (mean ± standard deviation). The respective Cu/(In + Ga) and Ga/(In + Ga) ratios were 0.94 ± 0.03 and 0.26 ± 0.02, indicating their appropriateness for high-efficiency CIGS absorbers. Additional measurements taken at the left, center, and right regions of the sample indicate variations within ±0.03, confirming consistent lateral compositional uniformity.

The final thickness of the CIGS film was achieved under variable current densities and pulse timing conditions. The thicknesses of the as-deposited and annealed films were determined by cross-sectional SEM analysis and corroborated by stylus profilometry. The thickness of the CIGS layer was approximately 1.4 to 1.6 µm, which is expected to be adequate to absorb 97% of the incident light.

3.5. Post-Deposition Thermal Annealing

Thermal annealing is an essential step for optimizing the atomic structure of the deposit, removing recombination defects, and ensuring uniform composition throughout the sample [40–44]. The post-treatment conditions were the same as those established for the CIGS layer in the prior study. The decreased annealing time was derived from our

previously published research [3,6], in which the annealing process for CIGS layers was methodically examined and optimized, as well as from a limited set of supplementary experiments conducted from 2 h to 45 min in this study to refine the annealing parameters for films produced from the diluted electrolyte.

Table 2 depicts changes in the deposit composition, evaluated before and after annealing.

Table 2. Plated film atomic compositions before and after annealing as measured by XRD analysis. Plating conditions are identical to those listed in the caption of Figure 6.

Element	Before Annealing [Atomic %]	After Annealing [Atomic %]
Copper	21.8%	25.1%
Indium	19.5%	17%
Gallium	6.9%	7.7%
Selenium	51.8%	50.2%

4. Device Characterization

4.1. XRD Diffraction Analysis of CIGS Electrodeposits

The CIGS absorber layer annealing process was conducted for thirty minutes in an argon environment, as illustrated in Figure 8, followed by crystallographic and morphological assessment using XRD. The clarity and intensity of the diffraction peaks were enhanced in the deposits produced from the lower-concentration electrolyte using the pulsing current method (Figure 8). At 28.34, the most prominent diffraction peak emerges, signifying that the necessary crystallography has been achieved.

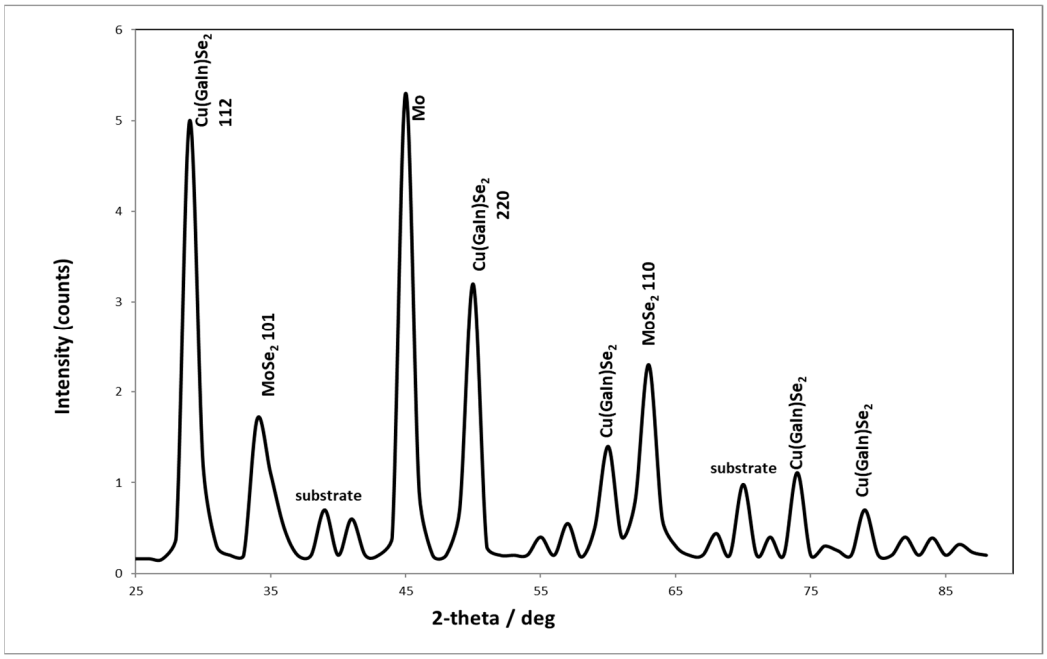


Figure 8. XRD of electrodeposited CIGS layer after the annealing process. The deposition pulsing current is 4.2 mA/cm^2 with 50 msec on and 50 msec off. The electrolyte from which the CIGS was deposited consisted of 0.47 mM $CuCl_2 \cdot H_2O$, 0.40 mM $InCl_3$, 0.71 mM H_2SeO_3, and 0.55 mM $GaCl_3$, supporting the bath. 0.65 M LiCl was added as a supporting electrolyte, and pHydrion was added to buffer the electrolyte to pH = 2.

The XRD patterns of the annealed CIGS films deposited from the dilute electrolyte exhibit a prominent diffraction peak at approximately 28.4° 2θ, which corresponds to

the (112) plane of the chalcopyrite Cu(In,Ga)Se_2 phase, as identified in the JCPDS/ICDD database. This primary (112) reflection verifies the development of the anticipated CIGS absorber architecture. Additional minor peaks at higher angles, corresponding to the (204)/(220) and (312)/(116) reflections, are also detected with relative intensities consistent with the standard CIGS pattern, indicating a polycrystalline film with a predominant (112) orientation. No discernible peaks corresponding to Cu–Se or In/Ga–Se secondary phases are observed within the measurement's sensitivity, indicating that the films are predominantly single-phase CIGS. The relatively pointed and prominent (112) peak at 28.34° further indicates enhanced crystallinity in films deposited at lower current densities and shorter pulse-off durations, consistent with the improved morphological quality described in the preceding section.

4.2. Device Efficiency

Nine entirely fabricated CIGS devices were examined. The highest efficiency was 1.9% with medium pulse timing (100 ms on/off), while 1.2% was recorded with long pulse timing (250 ms on/off). In contrast, the short pulse timing (50 ms on/off) resulted in an efficiency of 4.72%, which is attributed to transient current effects.

CIGS devices constructed from films produced with the diluted concentration electrolyte using the pulsed current method exhibited a current–voltage (I–V) efficiency of approximately 4.7% (Figure 9). The device characterization was conducted under AM1.5 illumination at 1000 W/m^2. The short-circuit current was approximately 18.4 mA/cm^2, the open-circuit voltage was approximately 0.29 V, and the device's fill factor was approximately 49.5% (Figures 9 and 10). The series RS and shunt RSh resistances were 7.92 Ω and 1092 Ω, respectively (Table 3).

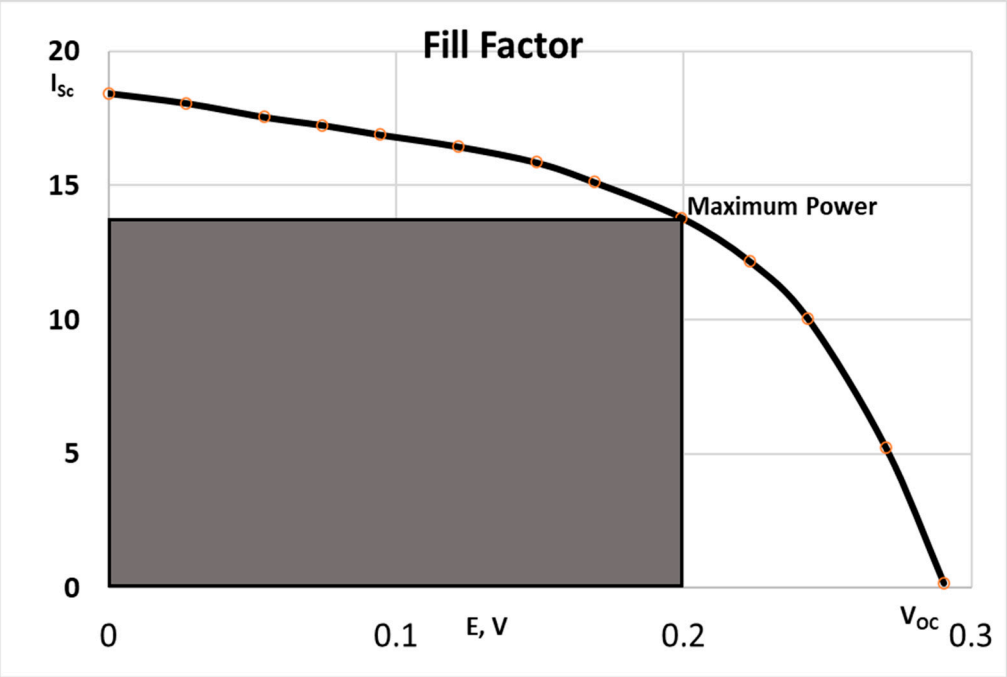


Figure 9. Current–voltage (I–V) characteristics of SS/Mo/CIGS/CdS/i-ZnO/Al: ZnO structure (±1 standard deviation based on repeated measurements).

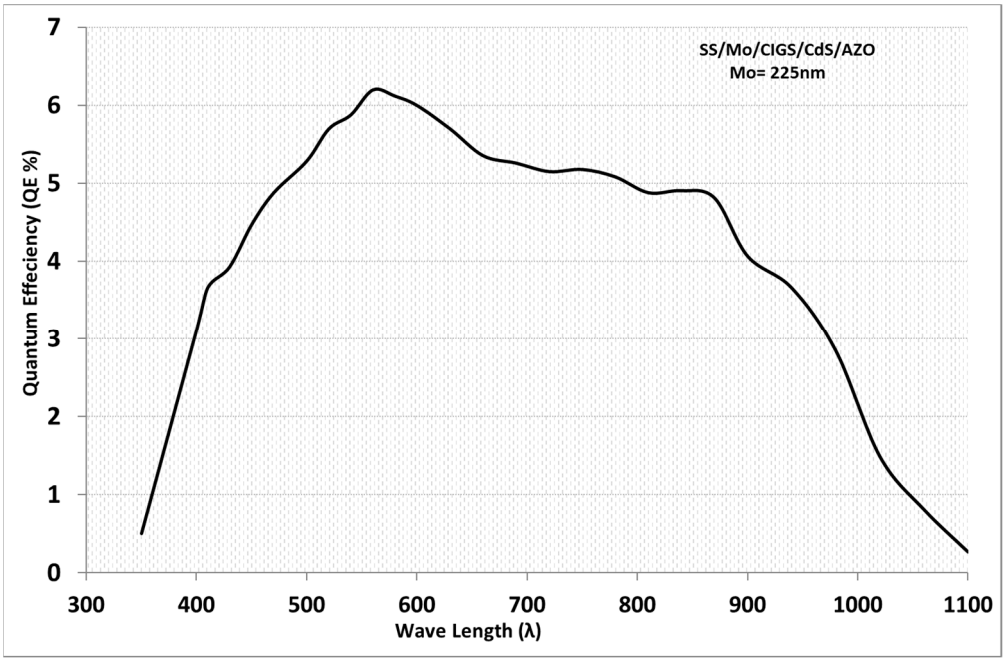


Figure 10. Quantum efficiency characteristics of SS/Mo/CIGS/CdS/i-ZnO/Al: ZnO structure (±1 standard deviation based on repeated measurements).

Table 3. I–V and diode parameters (AM 1.5 G, 100 mW/cm^2, cell area = 0.3167 cm^2).

Parameter	Symbol	Example Value	Unit	How It's Obtained/Comment
Series resistance	Rs	8.2	Ω·cm^2	from slope of illuminated I–V near Voc
Shunt resistance	Rsh	810	Ω·cm^2	from slope near Jsc
Diode ideality factor	*n*	1.8	–	from dark I–V fit to single-diode equation
"Ideal" FF (no Rs/Rsh)	FF_0	68.80%	–	calculated from Voc, *n*
Series-resistance loss in FF	ΔFF	≈19.3 percentage points	–	FF drops from 68.8% to 49.1%
Power loss due to Rs	$P_{loss,Rs}$	≈0.0019 W/cm^2	–	≈1.9% absolute loss in η

Figure 10 illustrates the quantum efficiency of the CIGS solar device under illumination at 1000 W/m^2. According to this characterization test, CIGS absorbs more photons in the visible spectrum than at longer wavelengths. The quantum efficiency decreased due to recombination in the distorted crystal structure. The measured value of 1.13 eV aligns with the computed band gap. The quantum efficiency was approximately 0.63 at the appropriate band gap [Figure 10].

Future research will address three critical aspects that were outside the scope of this investigation. Initially, the role of parasitic hydrogen evolution during CIGS electrodeposition from dilute electrolyte will be thoroughly examined by quantifying hydrogen evolution and optimizing pulse current parameters and electrolyte composition to reduce it while maintaining film density. Secondly, interface engineering at both the Mo/CIGS and CIGS/buffer interfaces will be investigated, encompassing the application of interfacial layers and surface treatments to enhance adhesion, minimize recombination, and ultimately convert improved film quality into increased device efficiencies. Third, additional refinement of stoichiometry control in diluted baths will be achieved by integrating meticulous bath management with comprehensive compositional mapping and modeling, thereby facilitating more accurate adjustment of the Cu/(In + Ga) and Ga/(In + Ga) ratios under the optimized pulsed current conditions established in this study.

5. Conclusions

This study carefully examined the pulse electrodeposition of CIGS absorber layers under various off-times, pulsing currents, and electrolyte concentrations. In this study, CIGS absorber layers were electrodeposited from diluted electrolytes under various pulsed current conditions to enhance film quality and device performance. Among the examined systems, diluted electrolytes paired with reduced pulsed current amplitudes and suitable on/off durations yielded smoother, more compact, and compositionally uniform CIGS deposits relative to higher current configurations. Furthermore, post-deposition annealing with reduced treatment durations was sufficient to produce well-crystallized, uniform layers, preventing excessive grain growth or film deterioration. Following completion of the device stack, these optimized conditions yielded CIGS solar cells with satisfactory efficiency, confirming that precise adjustment of electrolyte dilution, pulse current parameters, and annealing duration is essential for producing high-quality absorber layers and ensuring consistent device performance.

It was established that, unlike earlier reported systems, the addition of metals from the gas phase during annealing is unnecessary, and the annealing duration in an argon atmosphere can be substantially reduced to approximately 30 min, compared with 2 h in the traditional approach.

The four elements exhibit uniform composition during pre-annealing, enabling a shorter annealing time. The optical properties of the CIGS device were identified and estimated. To improve crystallinity and morphology, additional research is required to examine the electrochemical behaviour associated with pulsing current deposition at transient current for the four species.

Funding: The research leading to these results has received funding from the Ministry of Higher Education, Research, and Innovation (MoHERI) of the Sultanate of Oman under the Block Funding Program. Agreement No. [MoHERI/BFP/ASU/2023/300].

Institutional Review Board Statement: Not applicable.

Data Availability Statement: Data are contained within the article.

Conflicts of Interest: The author declares no conflicts of interest. The funders had no role in the design of the study, in the collection, analyses, or interpretation of data; in the writing of the manuscript; or in the decision to publish the results.

References

1. Mandati, S.; Sarada, B.V. Electrodeposited Chalcopyrite $CuInGaSe_2$ Absorbers for Solar Energy Harvesting. *Mater. Sci. Energy Technol.* **2020**, *3*, 440–445. [CrossRef]
2. Chandran, R.; Panda, S.K.; Mallik, A. A short review on the advancements in electroplating of $CuInGaSe_2$ thin films. *Mater. Renew. Sustain. Energy* **2018**, *7*, 6. [CrossRef]
3. Saeed, M.; González Peña, O.I. Mass Transfer Study on Improved Chemistry for Electrodeposition of Copper Indium Gallium Selenide (CIGS) Compound for Photovoltaics Applications. *Nanomaterials* **2021**, *11*, 1222. [CrossRef]
4. Desarada, S.V.; Londhe, P.U.; Chaure, S.; Chaure, N.B. $CuInGaSe_2$ (CIGS) Thin Film on Flexible Mo Substrates from Non-Aqueous One-Step Electrodeposition Process. *J. Mater. Sci. Mater. Electron.* **2022**, *33*, 203–216. [CrossRef]
5. Duchatelet, A.; Sidali, T.; Loones, N.; Savidand, G.; Chassaing, E.; Lincot, D. 12.4% efficient $Cu(In,Ga)Se_2$ solar cell prepared from one-step electrodeposited Cu–In–Ga oxide precursor layer. *Sol. Energy Mater. Sol. Cells* **2013**, *119*, 241–245. [CrossRef]
6. Saeed, M.; González Peña, O.I. Introducing a Dilute Single Bath for the Electrodeposition of $Cu_2(ZnSn)(S)_4$ for Smooth Layers. *Electrochem* **2024**, *5*, 354–369. [CrossRef]
7. Ledesma-Juárez, A.; Fernandez, A.M. Preparation and Characterization of Cu–In–Ga–Se Thin Films by the Electrodeposition Technique Using Different Metal Salts and Substrates. *J. Mater. Sci. Mater. Electron.* **2023**, *34*, 1461. [CrossRef]
8. Su, Y.; Ho, W.; Lin, C.; Nieh, Y.; Liang, C. The Effects of the Morphology on the CIGS Thin Films Prepared by CuInGa Single Precursor. *Sol. Energy Mater. Sol. Cells* **2011**, *95*, 261–263. [CrossRef]

9. Vasekar, S.; Dhere, G. Effect of Sodium Addition on Cu-Deficient CuIn1−xGaxS2 Thin Film Solar Cells. *Sol. Energy Mater. Sol. Cells* **2009**, *93*, 69–73. [CrossRef]
10. Saeed, M. Electrochemical Fabrication of Thin Film Photovoltaic Devices (CIGS & CIGSS). Doctoral Dissertation, Case Western Reserve University, Cleveland, OH, USA, 2014. Available online: http://rave.ohiolink.edu/etdc/view?acc_num=case1396265882 (accessed on 1 January 2026).
11. Bhattacharya, R.N.; Oh, M.-K.; Kim, Y. CIGS-based Solar Cells Prepared from Electrodeposited Precursor Films. *Sol. Energy Mater. Sol. Cells* **2012**, *98*, 198–202. [CrossRef]
12. Li, B.; Zhao, A.; Xiang, D.; Peng, Z.; Yuan, Y.; Xing, Y.; Yao, L.; Bi, J.; Li, W. Smooth Cu electrodeposition for Cu(In, Ga)Se_2 thin-film solar cells: Dendritic clusters elimination by Ag buffer layer. *Energy Rep.* **2022**, *8*, 1847–1852. [CrossRef]
13. Dondapati, H.; Pradhan, A.K. Fabrication and Characterization of Electrochemically Deposited CuIn(Ga)Se_2 Solar Cells. *Nanomanufacturing* **2024**, *4*, 111–119. [CrossRef]
14. Ma, J.-S.; Yang, C.-Y.; Sung, J.-C.; Som, S.; Lu, C.-H. Preparation and Characterization of Cu(In,Ga)Se2 Thin Films via Direct Heating Selenium-Ion Containing Precursors. *Ceram. Int.* **2015**, *41*, 10980–10987. [CrossRef]
15. Machkih, K.; Oubaki, R.; Makha, M. A Review of CIGS Thin Film Semiconductor Deposition via Sputtering and Thermal Evaporation for Solar Cell Applications. *Coatings* **2024**, *14*, 1088. [CrossRef]
16. Ramanujam, J.; Singh, U.P. Copper Indium Gallium Selenide Based Solar Cells—A Review. *Energy Environ. Sci.* **2017**, *10*, 1306–1319. [CrossRef]
17. Bi, J.; Yao, L.; Ao, J.; Gao, S.; Sun, G.; He, Q.; Zhou, Z.; Sun, Y.; Zhang, Y. Pulse electrodeposition of copper on molybdenum for Cu(In,Ga)Se_2 and $Cu_2ZnSnSe_4$ solar cell applications. *J. Power Sources* **2016**, *326*, 211–219. [CrossRef]
18. Saeed, M.; González-Peña, O.I. Cu(In, Ga)(S, Se)$_2$ Electrodeposition and Characterizations Using Improved Electrolytes. *J. Appl. Electrochem.* **2025**, *55*, 943–955. [CrossRef]
19. Ledesma-Juárez, A.; Quintero-Guerrero, J.F.; Fernández, A.M. Fabrication and Characterization of Cu(In, Ga)Se_2 Thin Films by Electrodeposition: Optimization of the Thermal Treatment with Selenium and Mechanical Disturbance Technique. *Chalcogenide Lett.* **2025**, *22*, 97–108. [CrossRef]
20. Suhaimi, N.H.; Nur-E-Alam, M.; Yap, B.K.; Sobayel, K.; Miah, M.H.; Islam, M.A.; Tiong, S.K.; Das, N.; Khandakher, M.U.; Amin, N. Chronological progress in enhancing CIGS solar cell performance through window layer development: Fundamentals, synthesis, optimization. *Surf. Interfaces* **2024**, *54*, 105145. [CrossRef]
21. Park, M.; Ahn, S.; Yun, J.H.; Gwak, J.; Cho, A.; Ahn, S.; Shin, K.; Nam, D.; Cheong, H.; Yoon, K. Characteristics of Cu(In,Ga)Se_2 (CIGS) Thin Films Deposited by a Direct Solution Coating Process. *J. Alloys Compd.* **2012**, *513*, 68–74. [CrossRef]
22. Bi, J.; Gao, Q.; Ao, J.; Zhang, Z.; Sun, G.; Zhang, Y.; Liu, W.; Liu, F.; Sun, Y.; Xiang, D. Influence of Cu on Ga Diffusion during Post-Selenizing the Electrodeposited Cu/In/Ga Metallic Precursor Process. *Sol. Energy Mater. Sol. Cells* **2018**, *182*, 92–97. [CrossRef]
23. Oliveri, R.L.; Patella, B.; Di Pisa, F.; Mangione, A.; Aiello, G.; Inguanta, R. Fabrication of CZTSe/CIGS Nanowire Arrays by One-Step Electrodeposition for Solar-Cell Application. *Materials* **2021**, *14*, 2778. [CrossRef]
24. Alhammadi, S.; Park, H.; Kim, W.K. Optimization of Intrinsic ZnO Thickness in Cu(In,Ga)Se_2-Based Thin Film Solar Cells. *Materials* **2019**, *12*, 1365. [CrossRef]
25. Jackson, P.; Hariskos, D.; Lotter, E.; Paetel, S.; Wuerz, R.; Menner, R.; Wischmann, W.; Powalla, M. New world record efficiency for Cu(In,Ga)Se_2 thin-film solar cells beyond 20%. In *Progress in Photovoltaics: Research and Applications, Proceedings of the 25th EU PVSEC/WCPEC-5, Valencia, Spain, 6–10 September 2010*; Wiley Online Library: Hoboken, NJ, USA, 2011. [CrossRef]
26. Albiss, B.; Al-Widyan, M. Numerical Simulation, Preparation, and Evaluation of Cu(In, Ga)Se_2 (CIGS) Thin-Film Solar Cells. *ChemEngineering* **2023**, *7*, 87. [CrossRef]
27. Qing, G.; Ao, J.; Zhang, Y.; Zhang, Y.; Guo, J.; Sun, G.; Liu, W.; Liu, F.; Zhang, Y. Pulse Selenization in Cu(In,Ga)Se_2 Solar Cells: A Promising Approach to Achieve High Efficiency by Electrodeposition. *ACS Appl. Energy Mater.* **2021**, *4*, 8322–8329. [CrossRef]
28. Schumacher, S.; Botha, J.; Alberts, V. Photoluminescence Study of Potential Fluctuations in thin layers of $Cu(In_{0.75}Ga_{0.25})(S_ySe_{1-y})_2$. *J. Appl. Phys.* **2006**, *99*, 063508. [CrossRef]
29. Sharma, I.; Adari, K.V.K.; Biddika, L.; Borse, K. Synthesis and Characterization of Water-Based CIGS Ink for Photovoltaic Applications. *Discov. Mater.* **2024**, *4*, 76. [CrossRef]
30. Singh, P.; Das, S.; Mallik, A. A Detailed Investigation on the Phase Transformation Mechanism during Electroplating of Cu(In, Ga)Se_2 Films on FTO-Glass Substrates. *Sol. Energy* **2022**, *246*, 189–202. [CrossRef]
31. Chandran, R.; Behera, A.K.; Mallik, A. A Novel CISe/Ga-Se Two–Step Stack Approach to Electrodeposit Photovoltaic Quality Cu-Poor $CuInGaSe_2$ Thin Films. *Mater. Lett.* **2019**, *252*, 244–247. [CrossRef]
32. Chandran, R.; Behera, A.K.; Mallik, A. Composition Tuning of Single Step Electrodeposited $CuInSe_2$ Thin Films Using Sodium Dodecyl Sulfate as Additive. *J. Electron. Mater.* **2019**, *48*, 8129–8137. [CrossRef]
33. Lara-Lara, B.; Fernández, A.M. Growth improved of CIGS thin films by applying mechanical perturbations to the working electrode during the electrodeposition process. *Superlattices Microstruct.* **2019**, *128*, 144–150. [CrossRef]

34. Mandati, S.; Misra, P.; Sarada, B.V.; Rao, T.N. Copper Chalcopyrites for Solar Energy Applications. *Trans. Indian Inst. Met.* **2019**, *72*, 271–288. [CrossRef]
35. Regmi, G.; Ashok, A.; Chawla, P.; Semalti, P.; Velumani, S.; Sharma, S.N.; Castaneda, H. Perspectives of chalcopyrite-based CIGSe thin-film solar cell: A review. *J. Mater. Sci. Mater. Electron.* **2020**, *31*, 7286–7314. [CrossRef]
36. Saha, S.; Johnson, M.; Altayaran, F.; Wang, Y.; Wang, D.; Zhang, Q. Electrodeposition Fabrication of Chalcogenide Thin Films for Photovoltaic Applications. *Electrochem* **2020**, *1*, 286–321. [CrossRef]
37. Vigil-Galán, O.; Courel, M.; Andrade-Arvizu, J.A.; Sánchez, Y.; Espíndola-Rodríguez, M.; Saucedo, E.; Seuret-Jiménez, D.; Titsworth, M. Route towards low cost-high efficiency second generation solar cells: Current status and perspectives. *J. Mater. Sci. Mater. Electron.* **2015**, *26*, 5562–5573. [CrossRef]
38. Powalla, M.; Paetel, S.; Hariskos, D.; Wuerz, R.; Kessler, F.; Lechner, P.; Wischmann, W.; Friedlmeier, T.M. Advances in Cost-Efficient Thin-Film Photovoltaics Based on Cu(In,Ga)Se_2. *Engineering* **2017**, *3*, 445–451. [CrossRef]
39. Mandati, S.; Dey, S.R.; Joshi, S.V.; Bulusu, S.V. Cu(In,Ga)Se_2 Films with Branched Nanorod Architectures Fabricated by Economic and Environmental-friendly Pulse-reverse Electrodeposition Route. *ACS Sustain. Chem. Eng.* **2018**, *6*, 13787–13796. [CrossRef]
40. Wang, C.; Zhuang, D.; Zhao, M.; Ren, G.; Li, Y.; Wei, J.; Gong, Q.; Dong, L. Optimization of CuInGaSSe properties and CuInGaSSe/CdS interface quality for efficient solar cells processed with CuInGa precursors. *J. Power Sources* **2020**, *479*, 229105. [CrossRef]
41. Tong, H.; Kou, Z.; Zhao, M.; Zhuang, D.; Wang, C.; Li, Y. Influences of Mg concentration in ZnMgO film on energy band alignment at CIGSSe/$Zn_{1-x}Mg_xO$ interface and performances of CIGSSe solar cells. *Sol. Energy* **2022**, *246*, 216–223. [CrossRef]
42. Bouich, A.; Ullah, S.; Ullah, H.; Mollar, M.; Mari, B.; Touhami, M.E. Electrodeposited CdZnS/CdS/CIGS/Mo: Characterization and Solar Cell Performance. *JOM* **2020**, *72*, 615–620. [CrossRef]
43. Saïdia, H.; Alayaa, C.B.; Boujmila, M.F.; Durand, B.; Lazzari, J.L.; Bouaïcha, M. Physical Properties of Electrodeposited CIGS Films on Crystalline Silicon: Application for Photovoltaic Hetero-Junction. *Curr. Appl. Phys.* **2020**, *20*, 29–36. [CrossRef]
44. Sang, N.D.; Quang, P.H.; Tu, L.T.; Hop, D.T.B. Effect of Electrodeposition Potential on Composition and Morphology of CIGS Absorber Thin Film. *Bull. Mater. Sci.* **2013**, *36*, 735–741. [CrossRef]

Disclaimer/Publisher's Note: The statements, opinions and data contained in all publications are solely those of the individual author(s) and contributor(s) and not of MDPI and/or the editor(s). MDPI and/or the editor(s) disclaim responsibility for any injury to people or property resulting from any ideas, methods, instructions or products referred to in the content.